Synthetic lethality between the cohesin subunits *STAG1* and *STAG2* in diverse cancer contexts

Petra van der Lelij[1*], Simone Lieb[2*], Julian Jude[1], Gordana Wutz[1], Catarina P. Santos[3,4], Katrina Falkenberg[1], Andreas Schlattl[2], Jozef Ban[5], Raphaela Schwentner[5], Thomas Hoffmann[1], Heinrich Kovar[5,6], Francisco X. Real[3,4,7], Todd Waldman[8], Mark A. Pearson[2], Norbert Kraut[2], Jan-Michael Peters[1], Johannes Zuber[1] and Mark Petronczki[2#]

[1]Research Institute of Molecular Pathology (IMP), Vienna Biocenter (VBC), Campus-Vienna-Biocenter 1, 1030 Vienna, Austria

[2]Boehringer Ingelheim RCV, Dr. Boehringer Gasse 5-11, 1121 Vienna, Austria

[3]Spanish National Cancer Research Centre, Melchor Fernández Almagro 3, 28029 Madrid, Spain

[4]Centro de Investigación Biomédica en Red de Cáncer (CIBERONC), Av. Monforte de Lemos, 3-5. Pabellón 11. Planta 0 28029 Madrid, Spain

[5]Children's Cancer Research Institute, Zimmermannplatz 10, 1090 Vienna, Austria

[6]Department for Pediatrics, Medical University of Vienna, Spitalgasse 23, 1090 Vienna, Austria

[7]Department de Ciències Experimentals I de la Salut, Universitat Pompeu Fabra, Doctor Aiguader 88, 08003 Barcelona, Spain

[8]Lombardi Comprehensive Cancer center, Georgetown University School of Medicine, 3970 Reservoir Road NW, NRB E304, Washington, D.C., USA

*These authors contributed equally to this work

#Corresponding author: mark_paul.petronczki@boehringer-ingelheim.com

Keywords: cohesin, cancer, synthetic lethality, chromosomes, precision medicine

Abstract

Recent genome analyses have identified recurrent mutations in the cohesin complex in a wide range of human cancers. Here we demonstrate that the most frequently mutated subunit of the cohesin complex, *STAG2*, displays a strong synthetic lethal interaction with its paralog *STAG1*. Mechanistically, STAG1 loss abrogates sister chromatid cohesion in *STAG2* mutated but not in wild-type cells leading to mitotic catastrophe, defective cell division and apoptosis. STAG1 inactivation inhibits the proliferation of STAG2 mutated but not wild-type bladder cancer and Ewing sarcoma cell lines. Restoration of STAG2 expression in a mutated bladder cancer model alleviates the dependency on STAG1. Thus, STAG1 and STAG2 support sister chromatid cohesion to redundantly ensure cell survival. STAG1 represents a vulnerability of cancer cells carrying mutations in the major emerging tumor suppressor *STAG2* across different cancer contexts. Exploiting synthetic lethal interactions to target recurrent cohesin mutations in cancer, e.g. by inhibiting STAG1, holds the promise for the development of selective therapeutics.

Main text

Cohesin is a highly conserved ring-shaped protein complex that is thought to topologically embrace chromatid fibers (Peters & Nishiyama, 2012), which is essential for sister chromatid cohesion and chromosome segregation in eukaryotes. In addition, cohesin participates in DNA repair, genome organization and gene expression (Losada, 2014). The cohesin subunits SMC1, SMC3 and RAD21 (also called SCC1) comprise the core ring of the complex. A fourth universally conserved subunit, a HEAT repeat protein of the Scc3/STAG family, peripherally associates with the core cohesin ring by binding to RAD21 (Toth et al., 1999), and is required for the dynamic association of cohesin with chromatin (Hu et al., 2011; Murayama & Uhlmann, 2014). Human somatic cells express two paralogs of this protein, called STAG1 and STAG2 (Losada, Yokochi, Kobayashi, & Hirano, 2000; Sumara, Vorlaufer, Gieffers, Peters, & Peters, 2000).

Recent cancer genome studies identified recurrent mutations in cohesin subunits and regulators in approximately 7.3% of all human cancers (Lawrence et al., 2014; Leiserson et al., 2015; Solomon et al., 2011). *STAG2*, the most frequently mutated cohesin subunit, emerges as one of only 12 genes that are significantly mutated in 4 or more major human malignancies (Lawrence et al., 2014). *STAG2* mutations have been reported in ~6% of acute myeloid leukemias and myelodysplastic syndromes (Kon et al., 2013; Thota et al., 2014; Walter et al., 2012), 15-22% of Ewing's sarcomas (Brohl et al., 2014; Crompton et al., 2014; Tirode et al., 2014), and in up to 26% of bladder cancers of various stages and grades (Balbas-Martinez et al., 2013; Guo et al., 2013; Solomon et al., 2013; Taylor, Platt, Hurst, Thygesen, & Knowles, 2014). The deleterious nature of most *STAG2* mutations strongly suggests that the gene represents a new tumor suppressor (Hill, Kim, & Waldman, 2016). *STAG2* mutations were initially thought to promote tumorigenesis due to defects in sister chromatid cohesin leading to genome instability (Barber et al., 2008; Solomon et al., 2011). However, the vast majority of cohesin-mutated cancers are euploid (Balbas-Martinez et

3

al., 2013; Kon et al., 2013), indicating that cohesin mutations may promote tumorigenesis through altering different cohesin functions such as genome organization and transcriptional regulation (Galeev et al., 2016; Mazumdar et al., 2015; Mullenders et al., 2015; Viny et al., 2015). Regardless of the mechanisms driving cohesin mutant tumors, the recent success of poly(ADP-ribose) polymerase inhibitors in the treatment of *BRCA*-mutated ovarian and prostate cancer demonstrates that exploiting tumor suppressor loss by applying the concept of synthetic lethality in defined patient populations can impact clinical cancer care (Castro, Mateo, Olmos, & de Bono, 2016; G. Kim et al., 2015; Mirza et al., 2016; Oza et al., 2015). The estimated half a million individuals with *STAG2*-mutant malignancies would greatly profit from exploring specific dependencies of these cancers.

We hypothesized that STAG2 loss could alter the properties and function of the cohesin complex leading to unique vulnerabilities of *STAG2* mutated cells. To identify factors whose inactivation would be synthetic lethal with loss of STAG2 function, we first used CRISPR/Cas9 to inactivate *STAG2* in near-diploid, chromosomally stable HCT 116 colon carcinoma cells (**Figure 1A**). Two clones, *STAG2*- 505c1 and 502c4, harboring deleterious mutations in *STAG2* and lacking detectable STAG2 protein expression were selected for analyses (**Figure 1-figure supplement 1** and **Supplementary file 1**). The isogenic parental and *STAG2*- HCT 116 cells were transfected with short-interfering RNA (siRNA) duplexes targeting 25 known cohesin subunits and regulators. After normalization to the non-target control siRNA (NTC), the effects of siRNA duplexes targeting individual genes were compared in parental and *STAG2*- cells. Depletion of the known essential cohesin regulator SGOL1, had a detrimental impact on viability of both parental and *STAG2*- cells. Remarkably, depletion of STAG1 strongly decreased cell viability in *STAG2*- cells, while being tolerated by the isogenic parental cells (**Figure 1B**). The pronounced selective effect of STAG1 depletion on *STAG2*- cells was confirmed in individual transfection experiments and colony formation assays (**Figure 1C,D,E**). Expression of an siRNA-resistant STAG1 transgene alleviated the anti-proliferative effect of STAG1 but not of SGOL1 siRNA duplexes in *STAG2*- HCT 116 cells

4

demonstrating the specificity of the siRNA treatment (**Figure 1-figure supplement 2**). Double depletion of STAG1 and STAG2 by siRNA in parental cells confirmed their synthetic lethal interaction (**Figure 1-figure supplement 3**). Co-depletion of p53 and STAG1 indicated that the dependency of *STAG2*- cells on STAG1 was independent of p53 (**Figure 1-figure supplement 4**). In contrast to the loss of essential cohesin subunits or regulators, depletion of STAG1 had no effect on cell viability in non-transformed telomerase-immortalized human retinal pigment epithelial cells (hTERT RPE-1) (**Figure 1-figure supplement 5**). This result is supported by a large-scale genetic loss-of-function study that found that neither *STAG1* nor *STAG2* is essential for the proliferation of hTERT-RPE1 cells (Hart et al., 2015). To corroborate our genetic interaction findings using an independent strategy, we introduced Cas9 into parental and *STAG2*- HCT 116 cells as well as KBM-7 leukemia cells for competition assays (**Figure 1F** and **Figure 1-figure supplement 1**). Transduction of lentiviruses co-expressing mCherry and single guide RNAs (sgRNAs) targeting essential cohesin subunit genes, such as RAD21 and SMC3, resulted in the rapid loss of the infected and mCherry-positive cells from the population irrespective of *STAG2* genotype (**Figure 1F**). In striking contrast, transduction with sgRNAs targeting *STAG1* caused the depletion of *STAG2*- HCT 116 and KBM-7 cells but not of their parental *STAG2* proficient counterparts (**Figure 1F**). Collectively, these experiments identify STAG1 as a vulnerability of *STAG2* mutated cells in engineered solid cancer and leukemia models. STAG1 inactivation has little if any impact on the viability and proliferation of *STAG2* wild-type cancer cells and non-transformed cells, but is essential for survival in the absence of STAG2.

To elucidate the mechanistic basis for this synthetic lethal interaction, we hypothesized that the combined loss of STAG1 and STAG2, in contrast to loss of either component alone, could severely impair cell division. Chromosome alignment and segregation during mitosis rely on sister chromatid cohesion, the central function of the cohesin complex (Peters & Nishiyama, 2012). Depletion of STAG1 resulted in an increase in the mitotic index and a prolongation of the duration of mitosis in

STAG2- but not wild-type cells (**Figure 2A** and **Figure 2-figure supplement 1**). Immunofluorescence microscopy revealed a failure to align chromosomes at the metaphase plate upon STAG1 loss in *STAG2-* cells (**Figure 2B**). In mitotic chromosome spread analysis *STAG2* inactivation caused a partial loss of centromeric cohesion in HCT 116 cells as previously reported (Canudas & Smith, 2009; J. S. Kim et al., 2016; Remeseiro et al., 2012; Solomon et al., 2011) (**Figure 2C**). Depletion of the essential centromeric cohesin protection factor SGOL1 resulted in a complete loss of sister chromatid cohesion in most chromosome spreads irrespective of *STAG2* genotype. In striking contrast, STAG1 depletion selectively abrogated sister chromatid cohesion in *STAG2-* but not parental cells (**Figure 2C,** single chromatids). The severe mitotic defects observed upon loss of STAG1 in *STAG2-* cells were accompanied by the emergence of aberrantly sized and shaped interphase nuclei (**Figure 2-figure supplement 2**) and by a progressive increase in apoptosis (**Figure 2D**). These results provide a mechanistic basis for the synthetic lethal interaction between *STAG1* and *STAG2*. *STAG1* inactivation abrogates sister chromatid cohesion exclusively in *STAG2-* cells resulting in catastrophic mitotic failure, abnormal cell division and apoptosis. To hold sister chromatids together, cohesin can tolerate the loss of either STAG1 or STAG2 alone but not the loss of both.

We next expanded our analysis to patient-derived *STAG2* mutations and *STAG2*-mutant cancer cell lines in order to investigate the disease relevance of the observed synthetic lethality (**Figure 3**). STAG1 depletion by siRNA abrogated both cell viability and sister chromatid cohesion in HCT 116 cell clones, in which three patient-derived deleterious mutations had been engineered into the *STAG2* locus (J. S. Kim et al., 2016), but not in parental HCT 116 cells (**Figure 3-figure supplement 1**). Among solid human cancers, *STAG2* mutational inactivation is most prevalent in urothelial bladder cancer and Ewing sarcoma. Therefore, we assembled a panel of 16 bladder cancer cell lines: 11 STAG2-positive, 3 with deleterious *STAG2* mutations (UM-UC-3, UM-UC-6 and VM-CUB-3), one in which *STAG2* was inactivated by CRISPR/Cas9 (UM-UC-5 *STAG2-*

6

505c6) (**Figure 3-figure supplement 2**), and two with no detectable STAG2 expression (LGWO1 and MGH-U3) (**Supplementary file 2**) (Balbas-Martinez et al., 2013; Solomon et al., 2013). The STAG2 protein expression status in the panel of bladder cancer cell lines was confirmed using immunoblotting (**Figure 3A**). siRNA experiments revealed that STAG2 status represented a predictive marker for the sensitivity to STAG1 depletion across the bladder cancer cell line panel. Whereas all cell lines were highly sensitive to depletion of the key mitotic kinase PLK1, STAG1 siRNA reduced cell viability in *STAG2*-negative bladder cancer cells but had little or no effect on STAG2-positive bladder cancer cell lines (**Figure 3B**). STAG1 depletion prevented colony formation and abolished sister chromatid cohesion selectively in *STAG2* mutated UM-UC-3 (F983fs) but not in *STAG2* wild-type UM-UC-5 bladder cancer cells (**Figure 3C,D**). In contrast, SGOL1 depletion abrogated cell growth and cohesion in both cell lines. Consistent with the results obtained in bladder cancer cells, *STAG2* mutation status also positively correlated with STAG1 dependency in a panel of four Ewing sarcoma cell lines (**Figure 3E,F** and **Supplementary file 2**) (Solomon et al., 2011; Tirode et al., 2014). Lentiviral transduction of a FLAG-STAG2 transgene into *STAG2* mutated UM-UC-3 bladder cancer cells resulted in the restoration of STAG2 expression, nuclear localization of the transgenic protein and its incorporation into the cohesin complex (**Figure 3-figure supplement 3**). Crucially, restoration of STAG2 expression alleviated the STAG1 dependency of UM-UC-3 cells providing a causal link between STAG2 loss and STAG1 dependency (**Figure 3G**). These results demonstrate that the synthetic lethal interaction between STAG1 and STAG2 that we discovered in isogenic cell pairs is recapitulated in disease-relevant bladder cancer and Ewing sarcoma cell models.

Here we identify *STAG1* as a strong genetic vulnerability of cells lacking the major emerging tumor suppressor STAG2 (**Figure 4**). The paralog dependency between STAG1 and STAG2 has recently also been reported in an independent study (Benedetti, Cereda, Monteverde, Desai, & Ciccarelli, 2017). We show that the synthetic lethal interaction between *STAG1* and *STAG2* is observed in

isogenic HCT 116 and KBM-7 cells as well as in bladder cancer and Ewing sarcoma cell lines. Thus, the genetic interaction between *STAG* paralogs is conserved in three major human malignancies: carcinoma, leukemia and sarcoma. Importantly, the finding that cancer cells harboring deleterious *STAG2* mutations remain exquisitely dependent on STAG1 demonstrates that this genetic vulnerability is maintained throughout the process of carcinogenesis and not bypassed by adaptive processes, such as the transcriptional activation of the germline-specific paralog *STAG3* (Pezzi et al., 2000; Prieto et al., 2001). Furthermore, expression analysis did not reveal upregulation of STAG1 protein or mRNA as a major compensatory mechanism for the loss of STAG2 function in cancer cell lines or patient tumors (**Figure 4-figure supplement 1**).

Our experiments strongly suggest that the loss of sister chromatid cohesion followed by aberrant cell division and cell death is the mechanistic basis underlying the synthetic lethality between *STAG1* and *STAG2* (**Figure 4**). Both paralogs associate with the cohesin complex in a mutually exclusive manner (Losada et al., 2000; Sumara et al., 2000). Although STAG1 and STAG2 may confer distinct functionalities to the cohesin complex (Canudas & Smith, 2009; Remeseiro et al., 2012), STAG1 and STAG2 containing complexes act redundantly to ensure sufficient sister chromatid cohesion to support cell division in human somatic cells. While the loss of one paralog is compatible with cell viability and proliferation, the loss of both paralogs abrogates cohesin's ability to hold sister chromatids together, which results in lethality. These mechanistic findings are consistent with previous studies that employed double siRNA depletion experiments to indicate functional redundancy between STAG1 and STAG2 in maintaining sister chromatid cohesion (Canudas & Smith, 2009; Hara et al., 2014; Remeseiro et al., 2012).

The fact that STAG1 inactivation has little or no effect on the proliferation of STAG2 proficient cells indicates that selective targeting of STAG1 could offer a large therapeutic window. Since STAG2 mRNA is expressed in all normal human tissues analyzed (**Figure 4-figure supplement 2**)

supports the hypothesis that selective inhibition of STAG1 function would indeed spare most non-cancerous tissues. Potential approaches for therapeutic targeting of STAG1 include the inhibition of the interaction between STAG1 and the cohesin ring subunit RAD21 (Hara et al., 2014) and the selective degradation of STAG1 using proteolysis-targeting chimera (PROTAC) technology (Deshaies, 2015). The high degree of homology between the STAG1 and its paralog STAG2 will be a key challenge to overcome. The mechanisms by which mutations in *STAG2* and other cohesin subunits drive tumorigenesis in solid and hematological tissues are not yet firmly established. Our work highlights the fact that such knowledge is not a prerequisite for the identification of selective vulnerabilities.

Both deleterious *STAG2* mutations and the loss of STAG2 expression are strong predictive biomarkers for STAG1 dependence in cell models and could be utilized for patient stratification in the future. Our work demonstrates that unique genetic dependencies of cohesin mutated cancer cells exist. Such vulnerabilities hold the promise to develop selective treatments for patients suffering from *STAG2* mutated cancer.

Author contributions

P.vdL. and S.L. performed most of the experiments, J.J. and K.F. performed KBM-7 experiments, G.W. performed initial HCT 116 experiments, J.B., R.S. and H.K. performed Ewing sarcoma experiments, C.P.S. and F.X.R. profiled bladder cancer cell lines, A. S. provided bioinformatic analyses, T.H. genetically engineered cell lines, T.W. provided HCT 116 patient mutation cell lines, S. L., M. A. P., N.K., P.vdL., J-M.P., J.Z. and M.P. designed the project and experiments, P.vdL. and M.P. wrote the manuscript. P.vdL., H.K., F.X.R., T.W., M.A.P., N.K., J-M.P., J.Z. and M.P. edited the manuscript. M.P. conceived and supervised the study.

Acknowledgements

Competing financial interests

S.L., A.S., M.A.P., N.K. and M.P. are employees of Boehringer Ingelheim RCV.

Materials and Methods

Antibodies. The following antibodies were used: C-term. pAb goat anti-STAG2 (Bethyl, A300-158A and A300-159A), N-term. mAb rabbit anti-STAG2 (Cell Signaling, 5882), full length pAb rabbit anti-STAG2 (Cell signaling, 4239), mouse anti-GAPDH (Abcam, ab8245), rabbit anti-STAG1 (Genetex, GTX129912), mouse anti-FLAG (Sigma, F3165 and F1804), mouse anti-p53 (Calbiochem, OP43), rabbit anti-H3pS10 (Millipore, 06570), FITC Conjugated mouse anti-Tubulin (Sigma, F2168), rabbit anti-SGOL1 (Peters laboratory ID A975M), SMC3 (Peters laboratory ID 845), mouse anti-RAD21 (Millipore, 05-908), rabbit anti-SMC1 (Bethyl A300-055A), and secondary rabbit (P0448), mouse (P0161) and goat (P0160) anti-IgG-HRP (all Dako).

CRISPR/Cas9 and cDNA transgene vectors. sgRNA sequences used in this study are listed in **Supplementary file 1**. The following lentiviral vectors were used to introduce mutations in *STAG2* in HCT 116 and UM-UC-5 cells: CRISPR STAG2 Hs0000077505_U6gRNA-Cas9-2A-GFP and CRISPR STAG2 Hs0000077502_U6gRNA-Cas9-2A-GFP (Sigma), CRISPR sgRNA STAG2_16 and sgRNA STAG2_19 were co-expressed from U6gRNA 16-U6gRNA 19-EF1αs-Thy1.1-P2A-neo to introduce mutations in *STAG2* in KBM-7 cells. HCT 116 stably expressing Cas9-GFP were obtained by lentiviral transduction with pLentiCRISPR-EF1αs-Cas9-P2A-GFP-PGK-puro. KBM-7 infected with dox-inducible Cas9 were obtained by sequential retroviral transduction with pWPXLd-EF1A-rtTA3-IRES-EcoRec-PGK-Puro and pSIN-TRE3G-Cas9-P2A-GFP PGK-Blast. pLVX-3xFLAG-STAG1r-IRES-Puro and pLVX-3xFLAG-STAG2r-IRES-Puro lentiviral vectors for siRNA-resistant transgene expression were generated by gene synthesis (GenScript) based on the STAG1 cDNA sequence NCBI NM_005862.2 and STAG2 cDNA sequence NCBI NM_001042749.2 followed by cloning into the parental pLVX vectors (Clontech). Silent nucleotide changes were introduced into the STAG1 and STAG2 coding sequences within the siRNA target

11

sequences to render the transgenes siRNA-resistant. For competition assays, U6-sgRNA-EF1αs-mCherry-P2A-neo lentiviral vectors were used.

Cell culture and lentiviral transduction. HCT 116 cells were cultured in McCoy's 5A w/glutamax medium supplemented with 10% fetal calf serum (FCS), KBM-7 cells were cultured in IMDM medium supplemented with 10% FCS, sodium butyrate, L-glutamine and antibiotics (all Invitrogen). hTERT RPE-1 cells were cultured in DMEM:F12 (ATCC: 30-2006) + 10% FCS + 0,01mg/ml hygromycin B. Bladder cancer cell lines UM-UC-5, UM-UC-6, UM-UC-18, LGWO1, and MGHU-3 were cultured in DMEM + 10% FCS w/NEAA, Glutamax and NaPyruvat, 5637, 639-V, 647-V, J82, JMSU-1, KU-19-19, RT4 T24, UM-UC-3 and VM-CUB-3 were cultured according to ATCC instructions. All Ewing sarcoma cell lines were cultured in RPMI + 10% FCS. Stable cell lines were generated by lentiviral transduction by use of one shot LentiX kit (Clontech) followed by puromycin selection (HCT 116: 2 μg/ml, UM-UC-3: 2 μg/ml, UM-UC-5: 3 μg/ml). Sources, STAG2 status and authentication information (STR fingerprinting) of cell lines used in this study are provided in **Supplementary file 2**. All cell lines were tested negatively for mycoplasma contamination.

siRNA transfection, cell viability, competition assay and apoptosis assay. For knockdown experiments, cells were transfected with ON-TARGETplus SMARTpool siRNA duplexes (Dharmacon) and the Lipofectamine RNAiMAX reagent according to the manufacturer's instructions (Invitrogen). HCT 116 chromosome spreads, apoptosis assay, immunoblotting, immunofluorescence and live cell imaging experiments were performed using a final siRNA concentration of 20 nM. Cell viability and crystal violet staining assays were performed using 10nM siRNA. hTERT RPE-1 cells and bladder cancer cells were transfected with 10 nM siRNA for cell viability assays, crystal violet staining and chromosome spreads. The UM-UC-3 FLAG-STAG2 cell line was transfected with 20 nM siRNA for immunoblotting. Ewing sarcoma cell lines were co-transfected with 50 nM ON-TARGETplus SMARTpool siRNAs (Dharmacon) plus pRetro-Super

(Brummelkamp, Bernards, & Agami, 2002) using Lipofectamin Plus reagent (Invitrogen). The next day cells were subjected to puromycin (1µg/ml) selection for 72 hours(Ban et al., 2014), and cultured for two additional days. Viability was determined using CellTiter-Glo (Promega), and by staining with crystal violet (Sigma, HT901). For sgRNA competition assays, Cas9-GFP was expressed constitutively (HCT 116) or was induced by doxycycline addition (KBM-7). mCherry and sgRNAs were introduced by lentiviral transduction. The fraction of mCherry-positive cells was determined at the indicated time points using a Guava easycyte flow cytometer (Millipore) and normalized to the first measurement and sequentially to control sgRNAs (non-targeting for HCT 116 and STAG2_19 for KBM-7). Apoptosis was analyzed using the IncuCyte Caspase-3/7 Apoptosis Assay (Essen BioScience).

Cell extracts for immunoblotting and FLAG-immunoprecipitation. Cell pellets were resuspended in extraction buffer (50 mM Tris Cl pH 8.0, 150 mM NaCl, 1% Nonidet P-40 supplemented with Complete protease inhibitor mix (Roche) and Phosphatase Inhibitor cocktails (Sigma, P5726 and P0044)); for **Figure 1-figure supplement 1** (KBM-7) and **Figure 3-figure supplement 1**, pellets were resuspended in (25mM Tris-HCl pH 7.5, 100mM NaCl, 5mM MgCl2, 0.2% NP-40, 10% glycerol, 1 mM NaF, Complete protease inhibitor mix (Roche), Benzonase (VWR)) and lysed on ice. For **Figure 1-figure supplement 2B** and **Figure 3-figure supplement 3C,** lysates were spun down for 10 minutes, followed by FLAG-immununoprecipitation using anti-FLAG M2-Agarose Affinity Gel (Sigma) for two hours and washing with lysis buffer. Input lysates and immunoprecipitates were resuspended in SDS sample buffer and heated to 95°C.

Immunofluorescence, live cell imaging and chromosome spreads. For immunofluorescence, cells were fixed with 4% paraformaldehyde for 15 min, permeabilized with 0.2% Triton X-100 in PBS for 10 min and blocked with 3% BSA in PBS containing 0.01% Triton X-100. Cells were incubated with primary and secondary antibody (Alexa 594, Molecular Probes), DNA was

counterstained with Hoechst 33342 (Molecular Probes H3570) and tubulin was sequentially stained with an FITC-conjugated antibody. Coverslips and chambers were mounted with ProLong Gold (Molecular Probes). Images were taken with an Axio Plan2/AxioCam microscope and processed with MrC5/Axiovision software (Zeiss). IncuCyte was used to record live cells, and duration of mitosis was determined by measuring the time from mitotic cell rounding until anaphase onset. Data analysis was performed with Microsoft Excel 2013 and GraphPad Prism 7. Significance levels were quantified using unpaired t test. For chromosome spread analysis, nocodazole was added to the medium for 60 minutes at 100 ng/ml. Cells were harvested and hypotonically swollen in 40% medium/60%tap water for 5 min at room temperature. Cells were fixed with freshly made Carnoy's solution (75% methanol, 25% acetic acid), and the fixative was changed three times. For spreading, cells in Carnoy's solution were dropped onto glass slides and dried. Slides were stained with 5% Giemsa (Merck) for 4 minutes, washed briefly in tap water and air dried. For chromosome spread analysis two independent slides were scored blindly for each condition.

Bioinformatic analysis of STAG1 and STAG2 mRNA expression. STAG2 mRNA expression in tumors (TCGA Research Network: http://cancergenome.nih.gov/) and STAG1 and STAG2 expression in normal human tissues (The Genotype-Tissue Expression (GTEx) project, www.gtexportal.org) (Consortium, 2013) were analyzed based on the data available from UCSC Xena version 2016-04-12. Expression levels correspond to transcripts per million (TPM) expression values. The downloaded values were log2(TPM+0.001) values which were transformed to TPM values before generating the figures. *STAG2* mutation data was downloaded from cBioPortal (Cerami et al., 2012; Gao et al., 2013) git repository in Sep. 2016. Samples were labeled as *STAG2* mutated if they carried an alteration resulting in an amino acid change in STAG2 (i.e. missense or nonsense point mutation or small insertion or deletion). Gene deletions or amplifications were not considered.

References

Balbas-Martinez, C., Sagrera, A., Carrillo-de-Santa-Pau, E., Earl, J., Marquez, M., Vazquez, M., . . . Real, F. X. (2013). Recurrent inactivation of STAG2 in bladder cancer is not associated with aneuploidy. *Nat Genet, 45*(12), 1464-1469. doi: 10.1038/ng.2799

Ban, J., Aryee, D. N., Fourtouna, A., van der Ent, W., Kauer, M., Niedan, S., . . . Kovar, H. (2014). Suppression of deacetylase SIRT1 mediates tumor-suppressive NOTCH response and offers a novel treatment option in metastatic Ewing sarcoma. *Cancer Res, 74*(22), 6578-6588. doi: 10.1158/0008-5472.CAN-14-1736

Barber, T. D., McManus, K., Yuen, K. W., Reis, M., Parmigiani, G., Shen, D., . . . Hieter, P. (2008). Chromatid cohesion defects may underlie chromosome instability in human colorectal cancers. *Proc Natl Acad Sci U S A, 105*(9), 3443-3448. doi: 10.1073/pnas.0712384105

Benedetti, L., Cereda, M., Monteverde, L., Desai, N., & Ciccarelli, F. D. (2017). Synthetic lethal interaction between the tumour suppressor STAG2 and its paralog STAG1. *Oncotarget, 8*(23), 37619-37632. doi: 10.18632/oncotarget.16838

Brohl, A. S., Solomon, D. A., Chang, W., Wang, J., Song, Y., Sindiri, S., . . . Khan, J. (2014). The genomic landscape of the Ewing Sarcoma family of tumors reveals recurrent STAG2 mutation. *PLoS Genet, 10*(7), e1004475. doi: 10.1371/journal.pgen.1004475

Brummelkamp, T. R., Bernards, R., & Agami, R. (2002). A system for stable expression of short interfering RNAs in mammalian cells. *Science, 296*(5567), 550-553. doi: 10.1126/science.1068999

Canudas, S., & Smith, S. (2009). Differential regulation of telomere and centromere cohesion by the Scc3 homologues SA1 and SA2, respectively, in human cells. *J Cell Biol, 187*(2), 165-173. doi: 10.1083/jcb.200903096

Castro, E., Mateo, J., Olmos, D., & de Bono, J. S. (2016). Targeting DNA Repair: The Role of PARP Inhibition in the Treatment of Castration-Resistant Prostate Cancer. *Cancer J, 22*(5), 353-356. doi: 10.1097/PPO.0000000000000219

Cerami, E., Gao, J., Dogrusoz, U., Gross, B. E., Sumer, S. O., Aksoy, B. A., . . . Schultz, N. (2012). The cBio cancer genomics portal: an open platform for exploring multidimensional cancer genomics data. *Cancer Discov, 2*(5), 401-404. doi: 10.1158/2159-8290.CD-12-0095

Consortium, G. T. (2013). The Genotype-Tissue Expression (GTEx) project. *Nat Genet, 45*(6), 580-585. doi: 10.1038/ng.2653

Crompton, B. D., Stewart, C., Taylor-Weiner, A., Alexe, G., Kurek, K. C., Calicchio, M. L., . . . Stegmaier, K. (2014). The genomic landscape of pediatric Ewing sarcoma. *Cancer Discov, 4*(11), 1326-1341. doi: 10.1158/2159-8290.CD-13-1037

Deshaies, R. J. (2015). Protein degradation: Prime time for PROTACs. *Nat Chem Biol, 11*(9), 634-635. doi: 10.1038/nchembio.1887

Galeev, R., Baudet, A., Kumar, P., Rundberg Nilsson, A., Nilsson, B., Soneji, S., . . . Larsson, J. (2016). Genome-wide RNAi Screen Identifies Cohesin Genes as Modifiers of Renewal and Differentiation in Human HSCs. *Cell Rep, 14*(12), 2988-3000. doi: 10.1016/j.celrep.2016.02.082

Gao, J., Aksoy, B. A., Dogrusoz, U., Dresdner, G., Gross, B., Sumer, S. O., . . . Schultz, N. (2013). Integrative analysis of complex cancer genomics and clinical profiles using the cBioPortal. *Sci Signal, 6*(269), pl1. doi: 10.1126/scisignal.2004088

Guo, G., Sun, X., Chen, C., Wu, S., Huang, P., Li, Z., . . . Cai, Z. (2013). Whole-genome and whole-exome sequencing of bladder cancer identifies frequent alterations in genes involved in sister chromatid cohesion and segregation. *Nat Genet, 45*(12), 1459-1463. doi: 10.1038/ng.2798

Hara, K., Zheng, G., Qu, Q., Liu, H., Ouyang, Z., Chen, Z., . . . Yu, H. (2014). Structure of cohesin subcomplex pinpoints direct shugoshin-Wapl antagonism in centromeric cohesion. *Nat Struct Mol Biol, 21*(10), 864-870. doi: 10.1038/nsmb.2880

Hart, T., Chandrashekhar, M., Aregger, M., Steinhart, Z., Brown, K. R., MacLeod, G., . . . Moffat, J. (2015). High-Resolution CRISPR Screens Reveal Fitness Genes and Genotype-Specific Cancer Liabilities. *Cell, 163*(6), 1515-1526. doi: 10.1016/j.cell.2015.11.015

Hill, V. K., Kim, J. S., & Waldman, T. (2016). Cohesin mutations in human cancer. *Biochim Biophys Acta, 1866*(1), 1-11. doi: 10.1016/j.bbcan.2016.05.002

Hu, B., Itoh, T., Mishra, A., Katoh, Y., Chan, K. L., Upcher, W., . . . Nasmyth, K. (2011). ATP hydrolysis is required for relocating cohesin from sites occupied by its Scc2/4 loading complex. *Curr Biol, 21*(1), 12-24. doi: 10.1016/j.cub.2010.12.004

Kim, G., Ison, G., McKee, A. E., Zhang, H., Tang, S., Gwise, T., . . . Pazdur, R. (2015). FDA Approval Summary: Olaparib Monotherapy in Patients with Deleterious Germline BRCA-Mutated Advanced Ovarian Cancer Treated with Three or More Lines of Chemotherapy. *Clin Cancer Res, 21*(19), 4257-4261. doi: 10.1158/1078-0432.CCR-15-0887

Kim, J. S., He, X., Orr, B., Wutz, G., Hill, V., Peters, J. M., . . . Waldman, T. (2016). Intact Cohesion, Anaphase, and Chromosome Segregation in Human Cells Harboring Tumor-Derived Mutations in STAG2. *PLoS Genet, 12*(2), e1005865. doi: 10.1371/journal.pgen.1005865

Kon, A., Shih, L. Y., Minamino, M., Sanada, M., Shiraishi, Y., Nagata, Y., . . . Ogawa, S. (2013). Recurrent mutations in multiple components of the cohesin complex in myeloid neoplasms. *Nat Genet, 45*(10), 1232-1237. doi: 10.1038/ng.2731

Lawrence, M. S., Stojanov, P., Mermel, C. H., Robinson, J. T., Garraway, L. A., Golub, T. R., . . . Getz, G. (2014). Discovery and saturation analysis of cancer genes across 21 tumour types. *Nature, 505*(7484), 495-501. doi: 10.1038/nature12912

Leiserson, M. D., Vandin, F., Wu, H. T., Dobson, J. R., Eldridge, J. V., Thomas, J. L., . . . Raphael, B. J. (2015). Pan-cancer network analysis identifies combinations of rare somatic mutations across pathways and protein complexes. *Nat Genet, 47*(2), 106-114. doi: 10.1038/ng.3168

Losada, A. (2014). Cohesin in cancer: chromosome segregation and beyond. *Nat Rev Cancer, 14*(6), 389-393. doi: 10.1038/nrc3743

Losada, A., Yokochi, T., Kobayashi, R., & Hirano, T. (2000). Identification and characterization of SA/Scc3p subunits in the Xenopus and human cohesin complexes. *J Cell Biol, 150*(3), 405-416.

Mazumdar, C., Shen, Y., Xavy, S., Zhao, F., Reinisch, A., Li, R., . . . Majeti, R. (2015). Leukemia-Associated Cohesin Mutants Dominantly Enforce Stem Cell Programs and Impair Human Hematopoietic Progenitor Differentiation. *Cell Stem Cell, 17*(6), 675-688. doi: 10.1016/j.stem.2015.09.017

Mirza, M. R., Monk, B. J., Herrstedt, J., Oza, A. M., Mahner, S., Redondo, A., . . . Investigators, E.-O. N. (2016). Niraparib Maintenance Therapy in Platinum-Sensitive, Recurrent Ovarian Cancer. *N Engl J Med, 375*(22), 2154-2164. doi: 10.1056/NEJMoa1611310

Mullenders, J., Aranda-Orgilles, B., Lhoumaud, P., Keller, M., Pae, J., Wang, K., . . . Aifantis, I. (2015). Cohesin loss alters adult hematopoietic stem cell homeostasis, leading to myeloproliferative neoplasms. *J Exp Med, 212*(11), 1833-1850. doi: 10.1084/jem.20151323

Murayama, Y., & Uhlmann, F. (2014). Biochemical reconstitution of topological DNA binding by the cohesin ring. *Nature, 505*(7483), 367-371. doi: 10.1038/nature12867

Oza, A. M., Cibula, D., Benzaquen, A. O., Poole, C., Mathijssen, R. H., Sonke, G. S., . . . Friedlander, M. (2015). Olaparib combined with chemotherapy for recurrent platinum-sensitive ovarian cancer: a randomised phase 2 trial. *Lancet Oncol, 16*(1), 87-97. doi: 10.1016/S1470-2045(14)71135-0

Peters, J. M., & Nishiyama, T. (2012). Sister chromatid cohesion. *Cold Spring Harb Perspect Biol, 4*(11). doi: 10.1101/cshperspect.a011130

Pezzi, N., Prieto, I., Kremer, L., Perez Jurado, L. A., Valero, C., Del Mazo, J., . . . Barbero, J. L. (2000). STAG3, a novel gene encoding a protein involved in meiotic chromosome pairing and location of STAG3-related genes flanking the Williams-Beuren syndrome deletion. *FASEB J, 14*(3), 581-592.

Prieto, I., Suja, J. A., Pezzi, N., Kremer, L., Martinez, A. C., Rufas, J. S., & Barbero, J. L. (2001). Mammalian STAG3 is a cohesin specific to sister chromatid arms in meiosis I. *Nat Cell Biol, 3*(8), 761-766. doi: 10.1038/35087082

Remeseiro, S., Cuadrado, A., Carretero, M., Martinez, P., Drosopoulos, W. C., Canamero, M., . . . Losada, A. (2012). Cohesin-SA1 deficiency drives aneuploidy and tumourigenesis in mice due to impaired replication of telomeres. *EMBO J, 31*(9), 2076-2089. doi: 10.1038/emboj.2012.11

Solomon, D. A., Kim, J. S., Bondaruk, J., Shariat, S. F., Wang, Z. F., Elkahloun, A. G., . . . Waldman, T. (2013). Frequent truncating mutations of STAG2 in bladder cancer. *Nat Genet, 45*(12), 1428-1430. doi: 10.1038/ng.2800

Solomon, D. A., Kim, T., Diaz-Martinez, L. A., Fair, J., Elkahloun, A. G., Harris, B. T., . . . Waldman, T. (2011). Mutational inactivation of STAG2 causes aneuploidy in human cancer. *Science, 333*(6045), 1039-1043. doi: 333/6045/1039 [pii]

10.1126/science.1203619

Sumara, I., Vorlaufer, E., Gieffers, C., Peters, B. H., & Peters, J. M. (2000). Characterization of vertebrate cohesin complexes and their regulation in prophase. *J Cell Biol, 151*(4), 749-762.

Taylor, C. F., Platt, F. M., Hurst, C. D., Thygesen, H. H., & Knowles, M. A. (2014). Frequent inactivating mutations of STAG2 in bladder cancer are associated with low tumour grade and stage and inversely related to chromosomal copy number changes. *Hum Mol Genet, 23*(8), 1964-1974. doi: 10.1093/hmg/ddt589

Thota, S., Viny, A. D., Makishima, H., Spitzer, B., Radivoyevitch, T., Przychodzen, B., . . . Maciejewski, J. P. (2014). Genetic alterations of the cohesin complex genes in myeloid malignancies. *Blood, 124*(11), 1790-1798. doi: 10.1182/blood-2014-04-567057

Tirode, F., Surdez, D., Ma, X., Parker, M., Le Deley, M. C., Bahrami, A., . . . the International Cancer Genome, C. (2014). Genomic landscape of Ewing sarcoma defines an aggressive subtype with co-association of STAG2 and TP53 mutations. *Cancer Discov, 4*(11), 1342-1353. doi: 10.1158/2159-8290.CD-14-0622

Toth, A., Ciosk, R., Uhlmann, F., Galova, M., Schleiffer, A., & Nasmyth, K. (1999). Yeast cohesin complex requires a conserved protein, Eco1p(Ctf7), to establish cohesion between sister chromatids during DNA replication. *Genes Dev, 13*(3), 320-333.

Viny, A. D., Ott, C. J., Spitzer, B., Rivas, M., Meydan, C., Papalexi, E., . . . Levine, R. L. (2015). Dose-dependent role of the cohesin complex in normal and malignant hematopoiesis. *J Exp Med, 212*(11), 1819-1832. doi: 10.1084/jem.20151317

Walter, M. J., Shen, D., Ding, L., Shao, J., Koboldt, D. C., Chen, K., . . . Graubert, T. A. (2012). Clonal architecture of secondary acute myeloid leukemia. *N Engl J Med, 366*(12), 1090-1098. doi: 10.1056/NEJMoa1106968
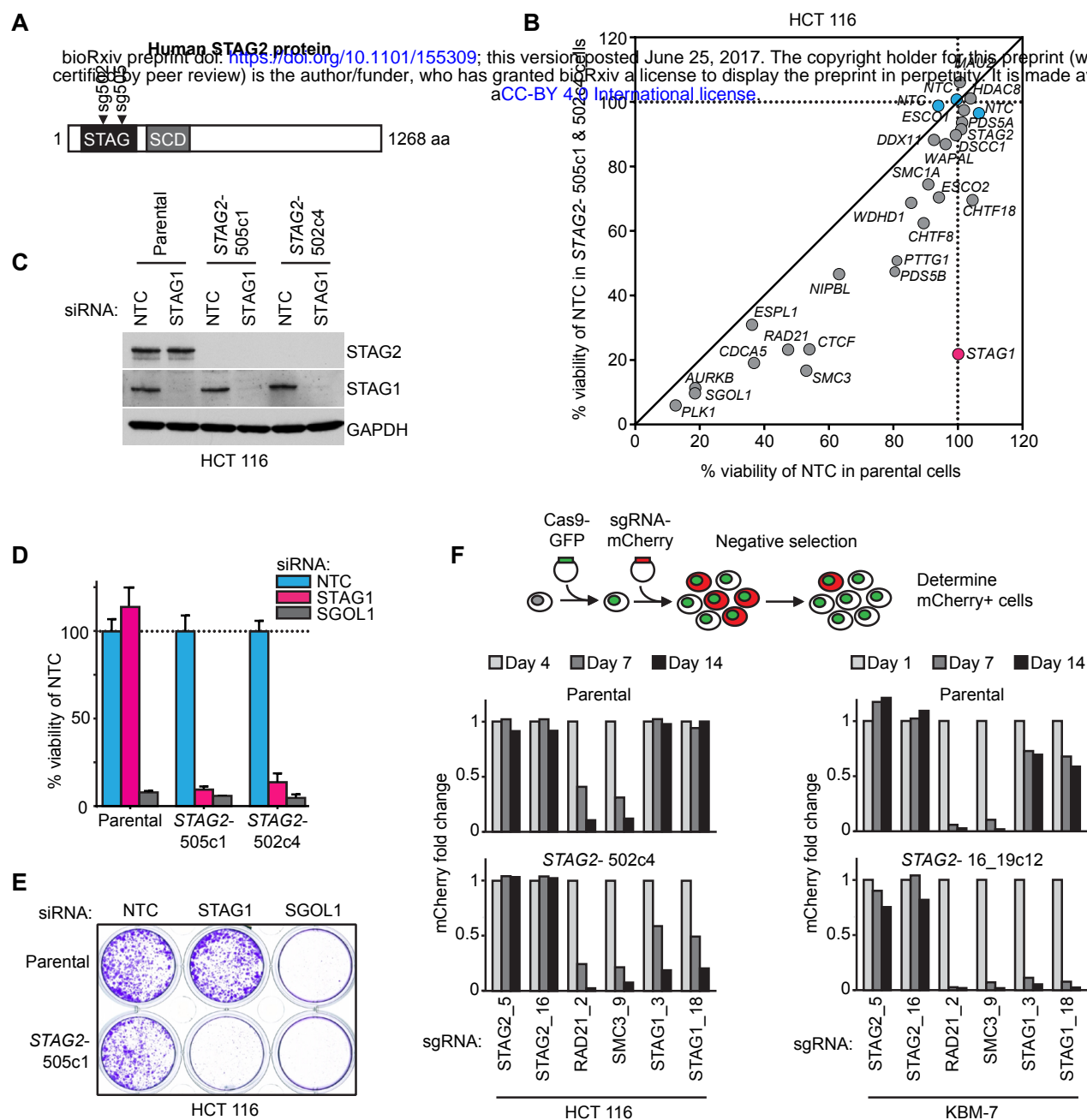
Figure 1. Identification of STAG1 as a synthetic lethal interaction of *STAG2* mutated cells. (**A**) Engineering of an isogenic HCT 116 cell model by CRISPR/Cas9-mediated inactivation of *STAG2*. The position of the sgRNAs used to create deleterious insertion and deletion mutations in the *STAG2* coding sequence is indicated. (**B**) Parental HCT 116 cells and two *STAG2* mutant clones (*STAG2-*) were subjected to an siRNA screen. Pools of 4 siRNA duplexes targeting 25 known cohesin subunits and regulators were transfected into the three cell lines. Cell viability was measured 7 days after transfection. Following normalization to non-target control (NTC) values, the average cell viability of siRNA pools in parental HCT 116 cells and two *STAG2-* clones was plotted against each other (n=2 or more independent experiments with 2 biological repeats each). (**C**) HCT 116 parental cells and *STAG2-* clones were transfected with the indicated siRNAs. Protein lysates were prepared 72 hours after transfection and analyzed by immunoblotting. (**D**) Cell viability was assessed 8 days after siRNA transfection using a metabolic assay (n=4 biological repeats, error bars denote standard deviation) and (**E**) using crystal violet staining. (**F**) Cas9-GFP expressing isogenic parental and *STAG2-* HCT 116 and KBM-7 cells were transduced with a lentivirus encoding mCherry and sgRNAs targeting the indicated genes. The percentage of mCherry-positive cells was determined over time by flow cytometry and normalized to the fraction of mCherry-positive cells at the first measurement and sequentially to a control sgRNA (n=1 experimental replicate).
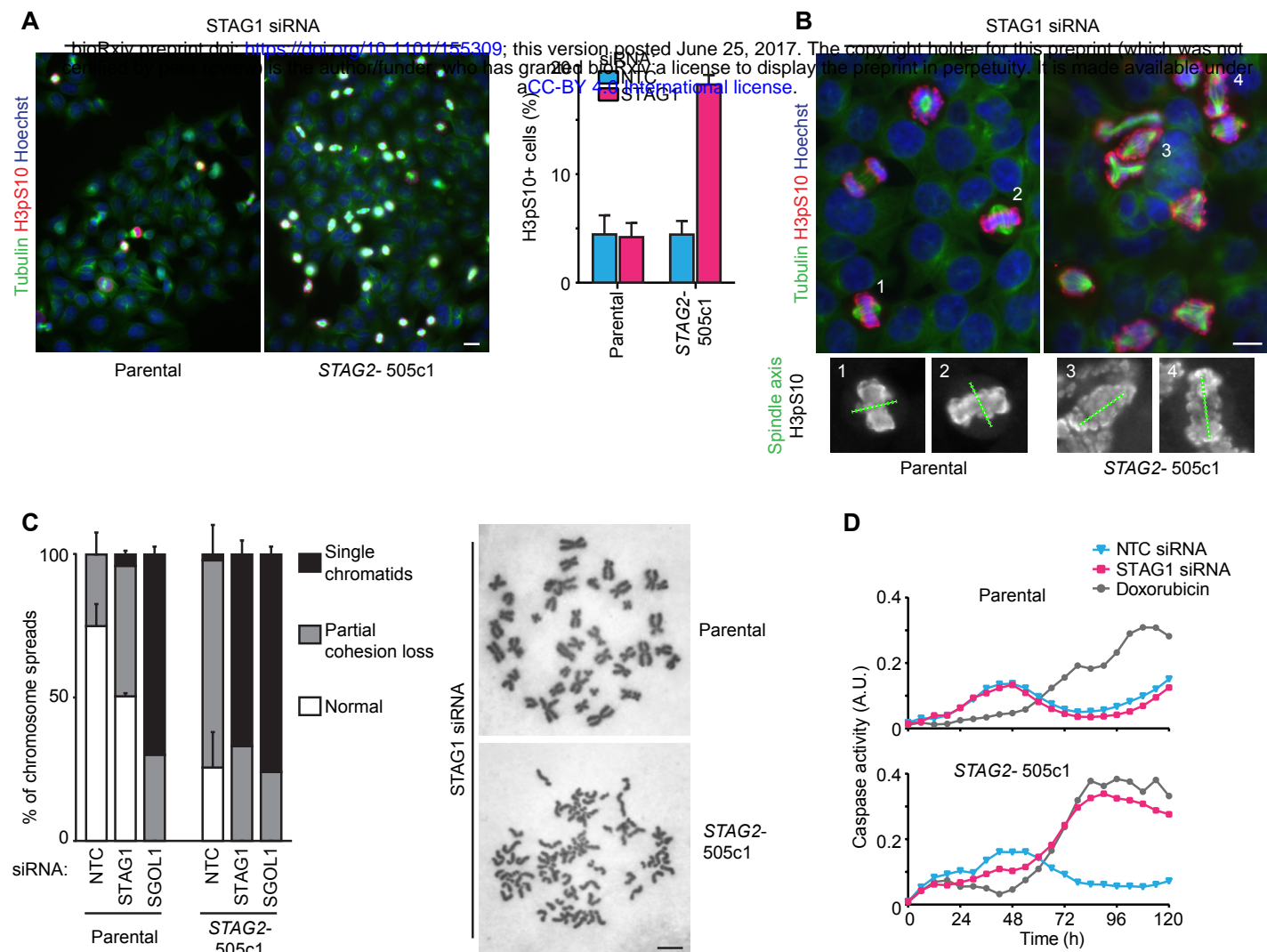
van der Lelij, Lieb *et al.* Figure 1

Figure 2. Loss of STAG1 function causes severe mitotic defects, abrogates sister chromatid cohesion and triggers apoptosis in *STAG2-* but not parental HCT 116 cells. (**A**) Parental and *STAG2-* 505c1 HCT 116 were transfected with NTC and STAG1 siRNA duplexes. Immunofluorescence analysis was performed 72 hours after transfection to determine the mitotic index by scoring the fraction of histone H3 phosphoSer10-positive (H3pS10+) cells (n≥1323 cells, error bars denote standard deviation of three independent experiments), and (**B**) to investigate mitotic spindle geometry and chromosome alignment. Cropped and magnified examples of chromosome alignment are shown in (B). Scale bars, 20 μm. (**C**) Giemsa-stained mitotic chromosome spreads were prepared 48 hours after transfection of parental and *STAG2-* HCT 116 cells with the indicated siRNA duplexes. The status of sister chromatid cohesion of individual metaphase spreads was categorized into normal, partial loss of cohesion or single chromatid phenotypes (n=100 spreads, error bars denote standard deviation of two independently analyzed slides). Scale bar, 10 μm. (**D**) Caspase activity was tracked over time using a live-cell caspase 3/7 substrate cleavage assay in parental and *STAG2-* 505c1 HCT 116 cells after transfection with the indicated siRNAs or after treatment with 0.3 μM doxorubicin at t = 0 hours (n=2 independent experiment with 4 biological repeats for NTC and STAG1 siRNA each and 1 biological repeat for doxorubicin each).

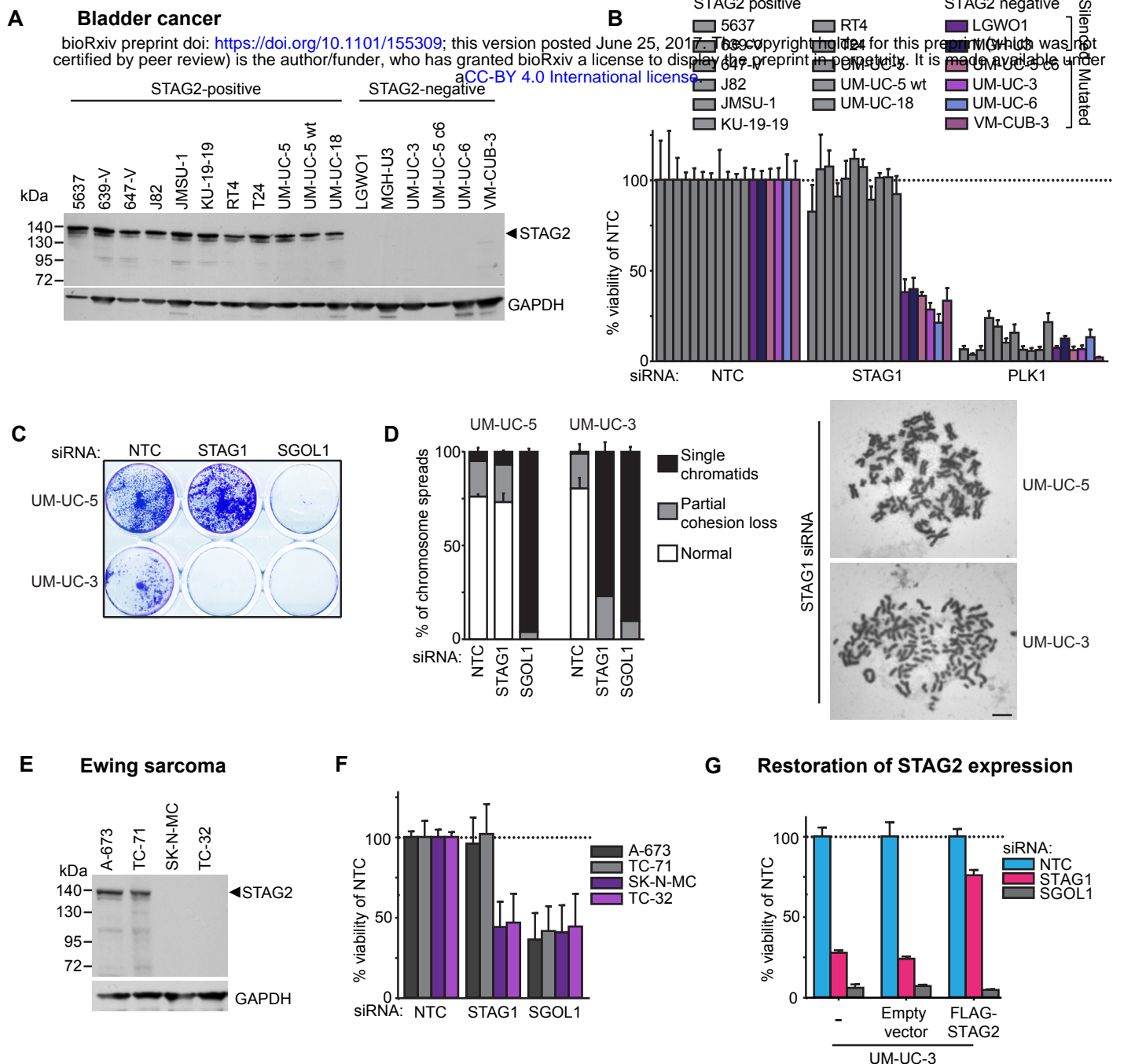van der Lelij, Lieb *et al.* Figure 2

Figure 3. The synthetic lethal interaction between *STAG1* and *STAG2* is manifested in disease-relevant bladder cancer and Ewing sarcoma cell lines. (**A**) The indicated bladder cancer cell lines were analyzed for STAG2 expression by immunoblotting. (**B**) The indicated bladder cancer cell lines were transfected with NTC, STAG1 and PLK1 siRNA duplexes. Viability was measured 7 or 10 days after transfection and normalized to the viability of NTC siRNA transfected cells (n=2 independent experiments with 5 biological repeats each, error bars denote standard deviation). (**C**) *STAG2* wild-type UM-UC-5 and *STAG2* mutated UM-UC-3 cells were transfected with NTC, STAG1 and SGOL1 siRNA duplexes. Colony formation was analyzed 7 days after transfection by crystal violet staining. (**D**) 72 hours after siRNA transfection into UM-UC-5 and UM-UC-3 cells, Giemsa-stained chromosome spreads were prepared and analyzed for sister chromatid cohesion phenotypes (n=100 spreads, error bars denote standard deviation of two independently analyzed slides). (**E**) The indicated Ewing sarcoma cell lines were analyzed for STAG2 protein expression by immunoblotting. (**F**) The indicated Ewing sarcoma cell lines were transfected with NTC, STAG1 and SGOL1 siRNA duplexes. Viability was measured 6 days after transfection and normalized to the viability of NTC siRNA transfected cells (n=3 independent experiments with 3 biological replicates each, error bars denote standard deviation). (**G**) *STAG2* mutated UM-UC-3 cells were transduced with a lentivirus encoding an siRNA-resistant FLAG-STAG2 transgene. Stably selected cell pools were subsequently transfected with NTC, STAG1 or SGOL1 siRNA duplexes. Viability was measured 7 days after transfection and normalized to the viability of NTC siRNA transfected cells (n=4 biological replicates, error bars denote standard deviation).
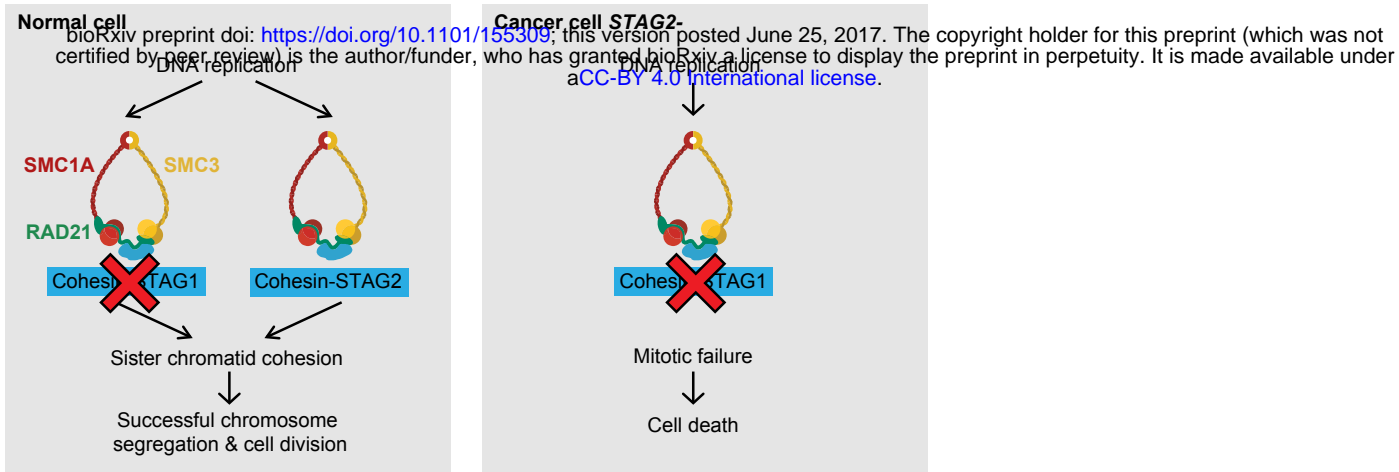
van der Lelij, Lieb *et al.* Figure 3

Figure 4. Model for the synthetic lethal interaction between *STAG1* and *STAG2*. In wild-type cells, both cohesin-STAG1 and cohesin-STAG2 complexes redundantly contribute to sister chromatid cohesion and successful cell division. Loss of STAG1 is tolerated in these cells as cohesin-STAG2 complexes alone suffice to support sister chromatid cohesion for cell division. In cancer cells in which *STAG2* is mutationally or transcriptionally inactivated, sister chromatid cohesion is entirely dependent on cohesin-STAG1 complexes. Inactivation of STAG1 in *STAG2* mutated cells therefore results in a loss of sister chromatid cohesion followed by mitotic failure and cell death.
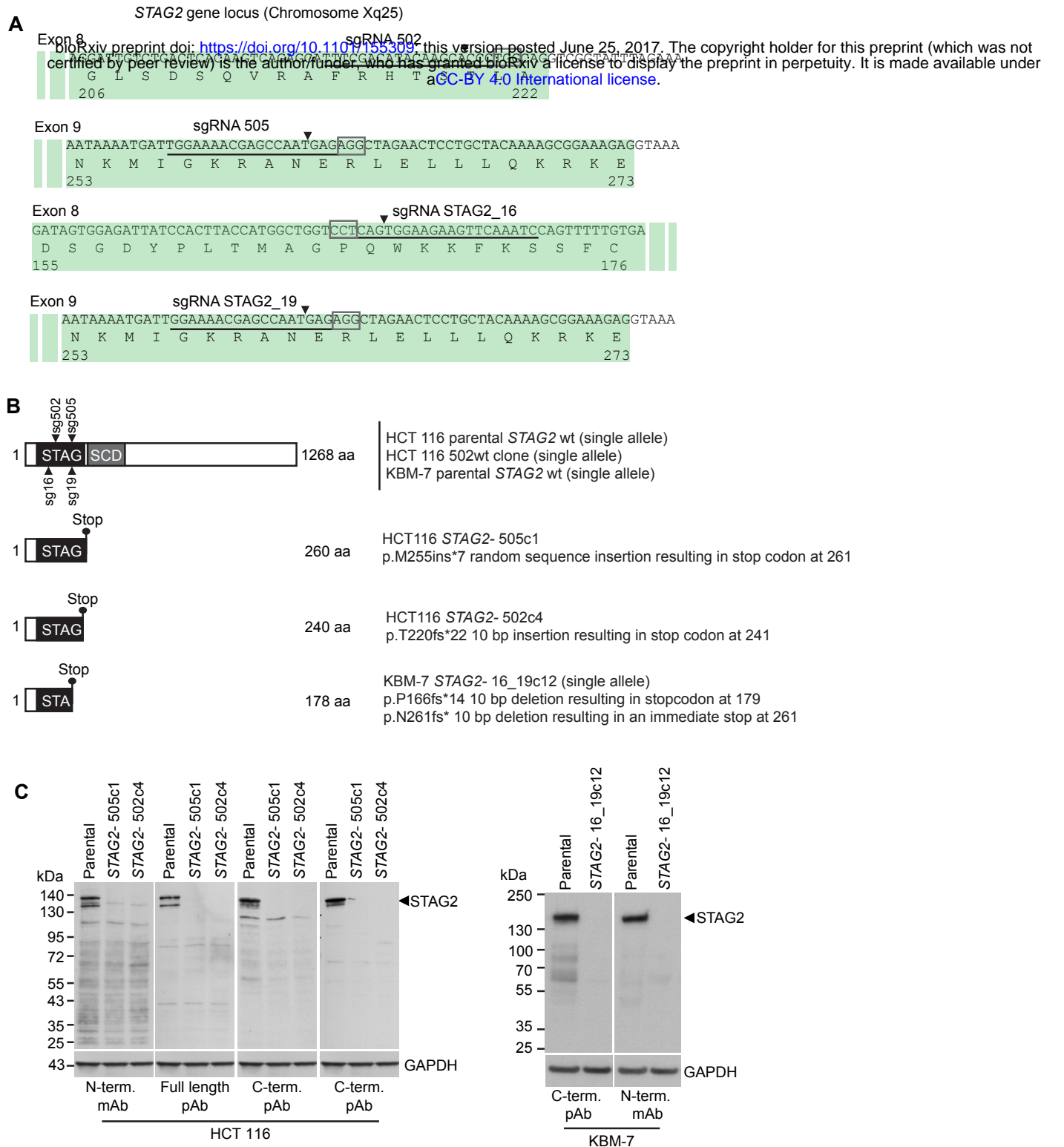
van der Lelij, Lieb *et al.* Figure 4

A

STAG2 gene locus (Chromosome Xq25)

Exon 8

sgRNA 502

```
G  L  S  D  S  Q  V  R  A  F  R  H  T  A
206                                    222
```

Exon 9   sgRNA 505

```
AATAAAATGATTGGAAAACGAGCCAATGAGAGGCTAGAACTCCTGCTACAAAAGCGGAAAGAGGTAAA
 N  K  M  I  G  K  R  A  N  E  R  L  E  L  L  L  Q  K  R  K  E
253                                                        273
```

Exon 8   sgRNA STAG2_16

```
GATAGTGGAGATTATCCACTTACCATGGCTGGTCCTCAGTGGAAGAAGTTCAAATCCAGTTTTTGTGA
 D  S  G  D  Y  P  L  T  M  A  G  P  Q  W  K  K  F  K  S  S  F  C
155                                                           176
```

Exon 9   sgRNA STAG2_19

```
AATAAAATGATTGGAAAACGAGCCAATGAGAGGCTAGAACTCCTGCTACAAAAGCGGAAAGAGGTAAA
 N  K  M  I  G  K  R  A  N  E  R  L  E  L  L  L  Q  K  R  K  E
253                                                        273
```

B

sg502 sg505
sg16 sg19

1 STAG SCD   1268 aa
HCT 116 parental STAG2 wt (single allele)
HCT 116 502wt clone (single allele)
KBM-7 parental STAG2 wt (single allele)

Stop
1 STAG   260 aa
HCT116 STAG2- 505c1
p.M255ins*7 random sequence insertion resulting in stop codon at 261

Stop
1 STAG   240 aa
HCT116 STAG2- 502c4
p.T220fs*22 10 bp insertion resulting in stop codon at 241

Stop
1 STA   178 aa
KBM-7 STAG2- 16_19c12 (single allele)
p.P166fs*14 10 bp deletion resulting in stopcodon at 179
p.N261fs* 10 bp deletion resulting in an immediate stop at 261

C

HCT 116 — N-term. mAb / Full length pAb / C-term. pAb / C-term. pAb
Lanes: Parental, STAG2- 505c1, STAG2- 502c4
kDa: 140, 130, 95, 72, 55, 43, 35, 25 — ◄STAG2
43 — GAPDH

KBM-7 — C-term. pAb / N-term. mAb
Lanes: Parental, STAG2- 16_19c12
kDa: 250, 130, 100, 70, 55, 35, 25 — ◄STAG2
GAPDH

Figure 1-figure supplement 1. Characterization of CRISPR/Cas9-generated STAG2 mutated clones used in this study. (**A**) Four different sgRNAs co-expressed with Cas9 from an all-in-one plasmid or a lentiviral vector were used to generate deleterious frameshift insertions or deletion mutations (indels) in STAG2 coding exons. sgRNAs sg502 and sg16 target exon 8 of STAG2, while sgRNAs sg505 and sg19 target exon 9 of the gene. Cognate sgRNA target sequences are underlined. Associated protospacer adjacent motifs (PAMs) are marked by boxes. The predicted Cas9 cleavage sites are marked by triangles. (**B**) CRISPR/Cas9-generated STAG2 indels in HCT 116 and KBM-7 cell clones as detected by Sanger sequencing. STAG2 is located on the X chromosome. Therefore, only one allele needed to be inactivated in HCT 116 (male) and KBM-7 (near-haploid) cells. (**C**) Protein lysates prepared from the indicated parental and mutant clones were analyzed for STAG2 protein expression by immunoblotting using antibodies directed against different STAG2 epitopes.

van der Lelij, Lieb et al. Figure 1-figure supplement 1
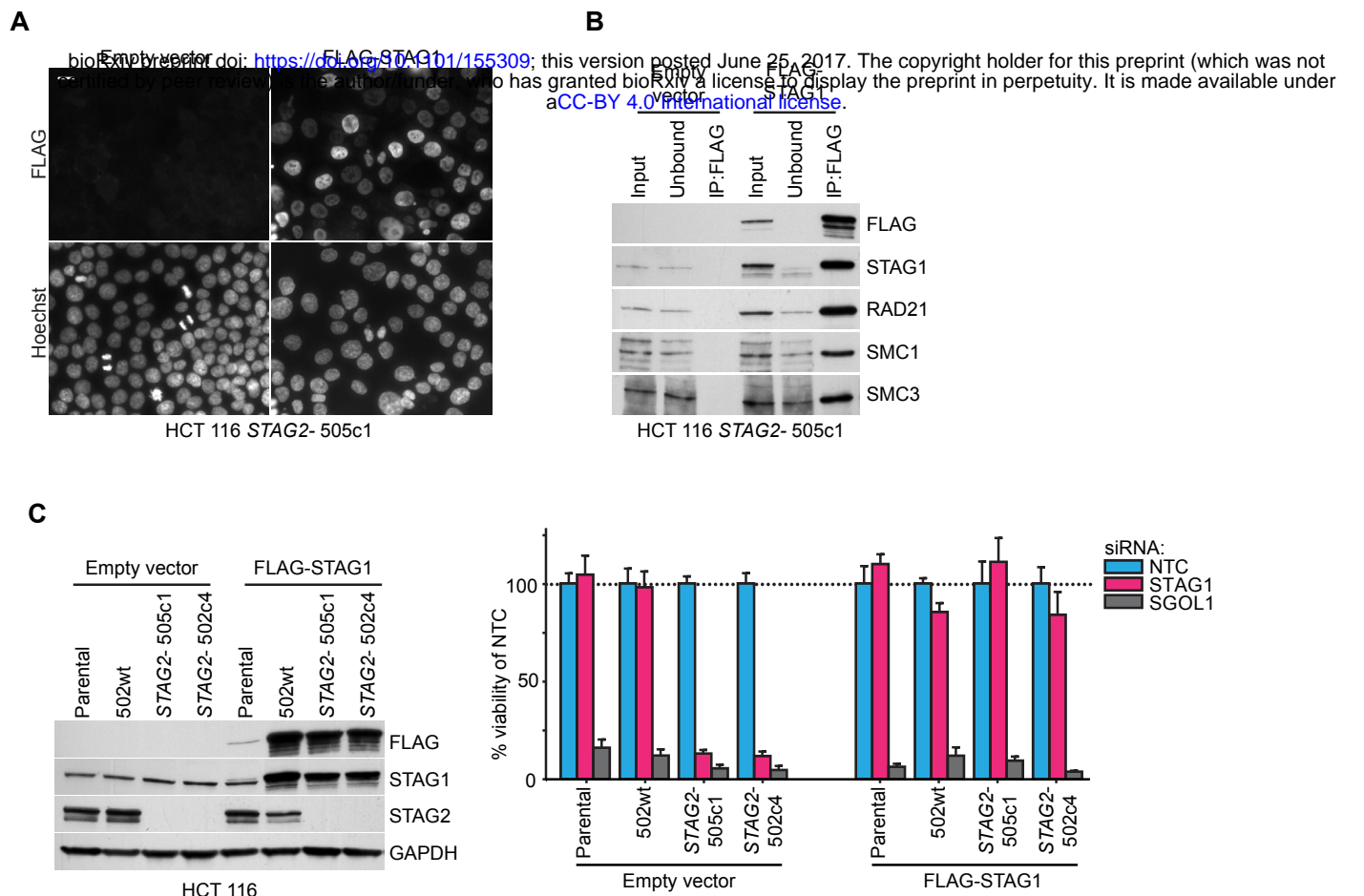
A

B

C

Figure 1-figure supplement 2. Rescue of the synthetic lethal interaction between *STAG1* and *STAG2* by expression of an siRNA-resistant FLAG-STAG1 transgene. HCT 116 parental cells, a *STAG2* wild-type clone (502wt), and two *STAG2-* clones (505c1 and 502c4) were transduced with a lentivirus encoding no transgene (empty vector) or an siRNA-resistant and 3xFLAG-tagged STAG1 transgene (FLAG-STAG1). Stably selected cell pools were used for the analysis. (**A**) Immunofluorescence analysis of FLAG-STAG1 transgene expression and nuclear localization in HCT 116 *STAG2-* 505c1 cells. Scale bar, 20 µm. (**B**) Protein extracts prepared from HCT 116 *STAG2-* 505c1 cells expressing no transgene (empty vector) or a FLAG-STAG1 transgene were subjected to anti-FLAG immunoprecipitation. The input, unbound and precipitated fractions were analyzed by immunoblotting. Co-precipitation of cohesin subunits was only detected in FLAG-STAG1 expressing cells indicating specific incorporation of the transgenic protein into the cohesin complex. (**C**) Protein extracts prepared from the indicated cell lines that were transduced with an empty vector or a FLAG-STAG1 transgene were analyzed by immunoblotting (left panel) and transfected with NTC, STAG1 and SGOL1 siRNA duplexes (right panel). Cell viability was measured 7 days after transfection and is plotted normalized to the viability of NTC siRNA transfected cells (n≥5 biological repeats, error bars denote standard deviation).

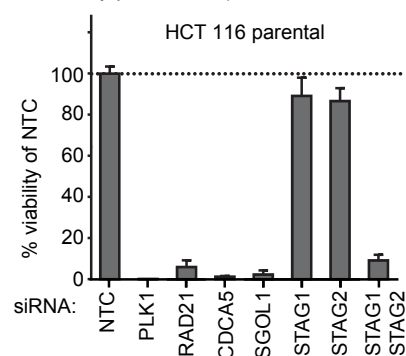van der Lelij, Lieb *et al.* Figure 1-figure supplement 2

Figure 1-figure supplement 3. Double depletion experiment confirms *STAG1/STAG2* synthetic lethality. (**A**) HCT 116 parental cells were co-transfected with NTC siRNA and siRNA duplexes targeting one of the following genes: NTC, PLK1, RAD21, CDCA5, SGOL1, STAG1 or STAG2. HCT 116 parental cells were also co-transfected with siRNA duplexes targeting STAG1 and STAG2. Cell viability was determined 8 days after transfection and is plotted normalized to cell viability of NTC siRNA-transfected cells (n=3 biological repeats, error bars denote standard deviation).

van der Lelij, Lieb *et al.* Figure 1-figure supplement 3
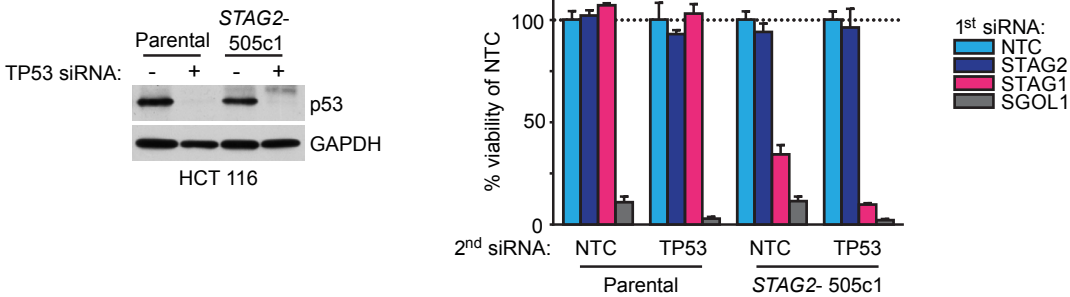
Figure 1-figure supplement 4. Double depletion experiments indicate that the *STAG1/STAG2* genetic interaction is independent of p53. Parental HCT 116 cells and *STAG2*- 505c1 cells were transfected with NTC (-) or TP53 (+) siRNA duplexes. Protein extracts were prepared 4 days after transfection and analyzed by immunoblotting (left panel). Parental HCT 116 cells and *STAG2*- 505c1 cells were co-transfected with the indicated siRNA duplexes (right panel). Cell viability was determined 8 days after transfection and is plotted normalized to the cell viability of NTC+NTC or NTC+TP53 siRNA-co-transfected cells (n=3 biological repeats, error bars denote standard deviation).

van der Lelij, Lieb *et al.* Figure 1-figure supplement 4
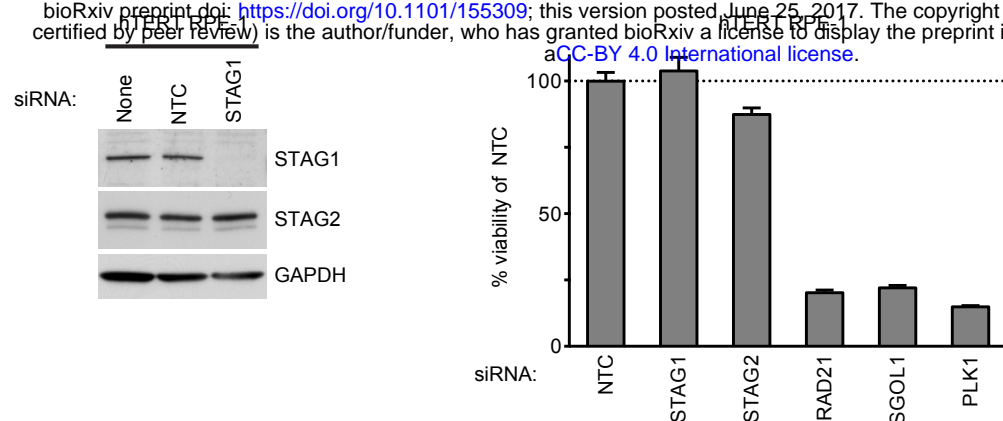
Figure 1-figure supplement 5. Depletion of STAG1 does not reduce viability in hTERT RPE-1 cells. Human telomerase-immortalized retinal pigment epithelial cells (hTERT RPE-1) were transfected with the indicated siRNA duplexes. Protein extracts were prepared 4 days after transfection and analyzed by immunoblotting (left panel). Cell viability was determined 5 days after transfection and is plotted normalized to the cell viability of NTC siRNA-transfected cells (n=2 independent experiments with 3 biological replicates each, error bars denote standard deviation).

van der Lelij, Lieb *et al.* Figure 1-figure supplement 5
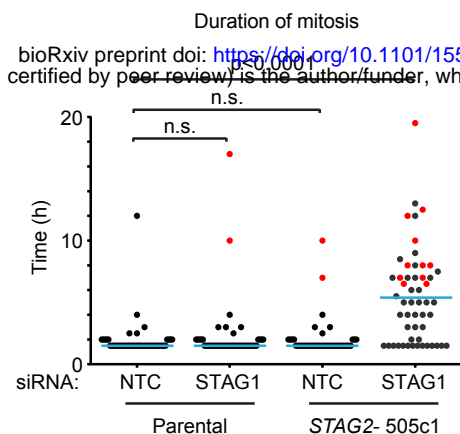
Figure 2-figure supplement 1. The depletion of STAG1 prolongs mitosis in *STAG2* mutated but not parental HCT 116 cells. Parental and *STAG2*- 505c1 HCT 116 were transfected with NTC and STAG1 siRNA duplexes. Cells were tracked from 0.5 to 72 hours (imaging interval 30 min) after transfection by bright-field live-cell imaging. The duration of mitosis (time elapsed from mitotic cell rounding to anaphase onset) and fate of individual cells were determined (n≥43 cells). The duration of mitosis of individual cells is plotted. Blue lines denote mean, red dots denote cells that died in mitosis. Significance levels were quantified using unpaired t test.

van der Lelij, Lieb *et al.* Figure 2-figure supplement 1
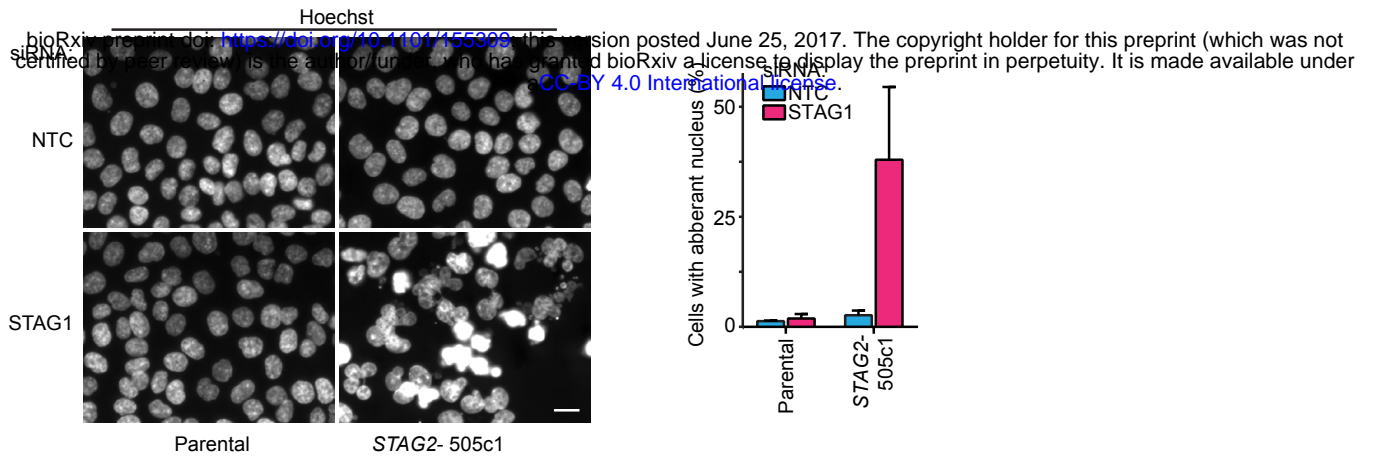
Figure 2-figure supplement 2. Aberrant nuclear morphology in *STAG2*-mutated but not parental HCT 116 cells upon depletion of STAG1. Parental and *STAG2*- 505c1 HCT 116 were transfected with NTC and STAG1 siRNA duplexes, fixed and stained with Hoechst 72 hours after transfection. Nuclei were scored for aberrant size (> 20 µm) or morphology (multi-nucleated cells and cells with polylobed nuclei; n≥ 612 nuclei, error bars denote standard deviation between two independent experiments).

van der Lelij, Lieb *et al.* Figure 2-figure supplement 2

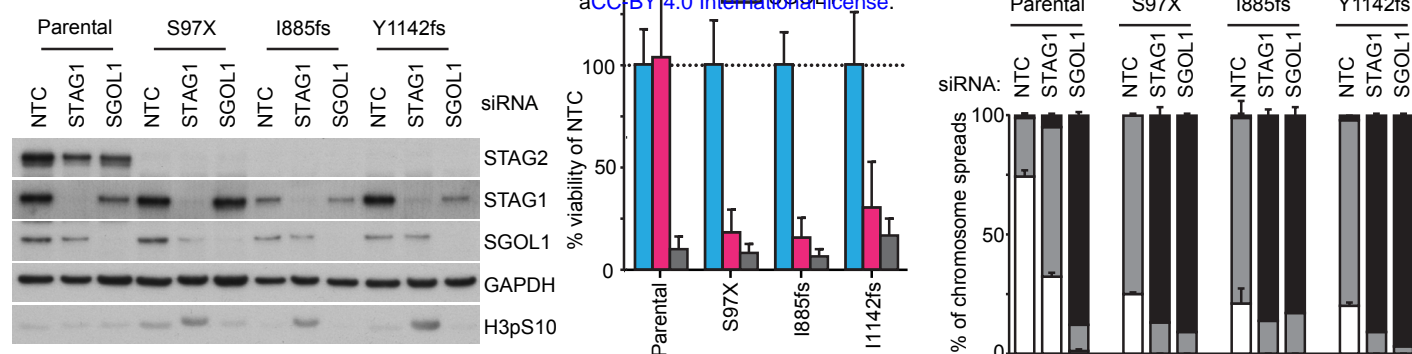**A HCT 116 *STAG2* cancer mutations**

Figure 3-figure supplement 1. Patient-derived *STAG2* mutations cause STAG1 dependency in engineered isogenic HCT 116 cells. HCT 116 cell lines engineered to harbor the indicated deleterious patient-derived *STAG2* mutations were transfected with NTC, STAG1 and SGOL1 siRNA duplexes. **A**, Protein extracts were prepared 48 hours after transfection and analyzed by immunoblotting. **B**, Cell viability was measured 7 days after siRNA transfection and plotted normalized to the viability of NTC-transfected cells (n=4 independent experiments with 5 biological repeats each, error bars denote standard deviation). **C**, Sister chromatid cohesion phenotypes were analyzed in Giemsa-stained mitotic chromosome spreads that were prepared 48 hours after siRNA transfection (n=100 chromosome spreads, error bars denote standard deviation between two independently analyzed slides).
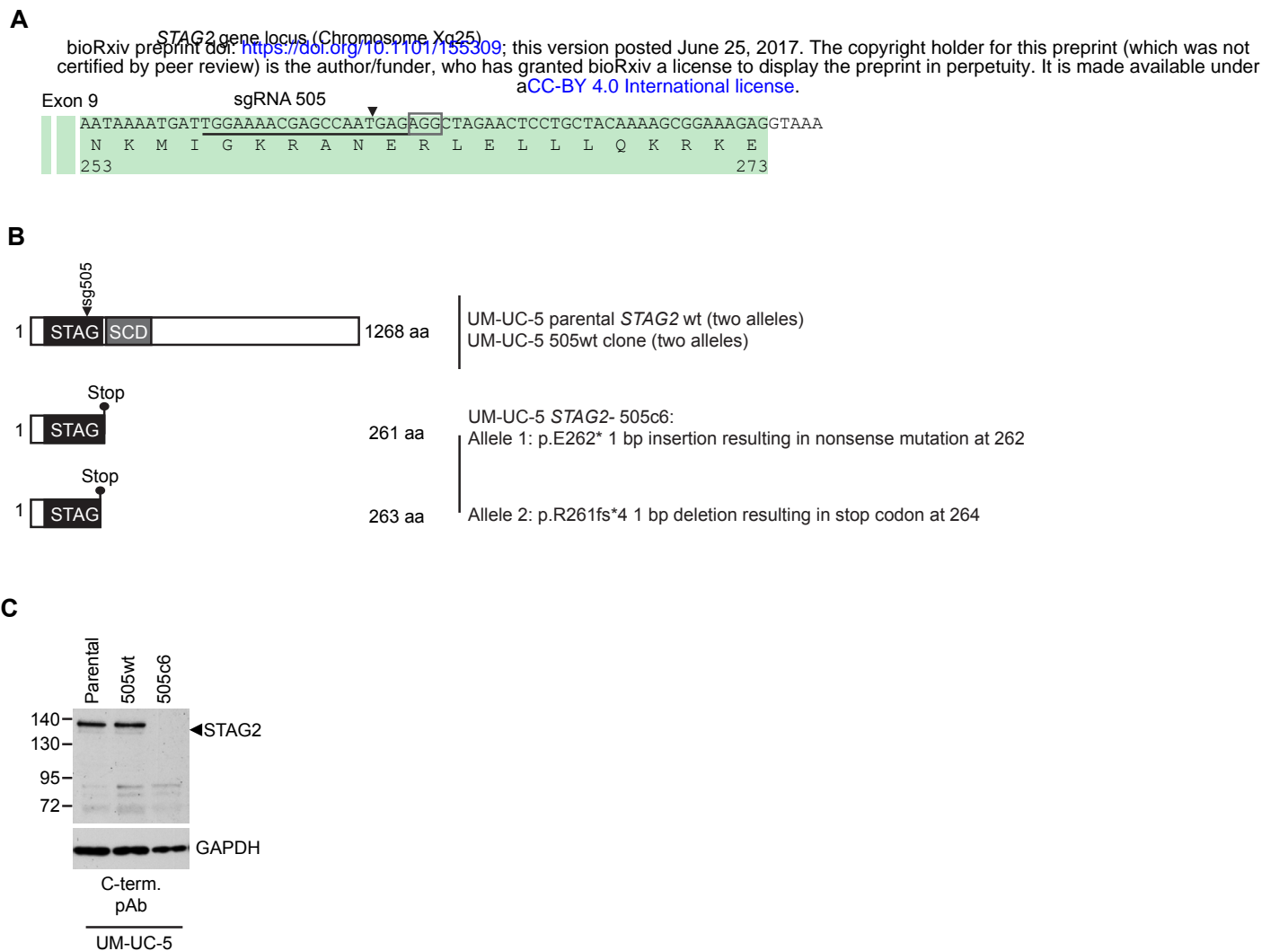
van der Lelij, Lieb *et al.* Figure 3-figure supplement 1

A

STAG2 gene locus (Chromosome Xq25)

Exon 9   sgRNA 505

```
AATAAAATGATTGGAAAACGAGCCAATGAGAGGCTAGAACTCCTGCTACAAAAGCGGAAAGAGGTAAA
    N  K  M  I  G  K  R  A  N  E  R  L  E  L  L  L  Q  K  R  K  E
    253                                                      273
```

B

sg505

| 1 | STAG | SCD | | 1268 aa | UM-UC-5 parental *STAG2* wt (two alleles)
UM-UC-5 505wt clone (two alleles) |

Stop

| 1 | STAG | | 261 aa | UM-UC-5 *STAG2*- 505c6:
Allele 1: p.E262* 1 bp insertion resulting in nonsense mutation at 262 |

Stop

| 1 | STAG | | 263 aa | Allele 2: p.R261fs*4 1 bp deletion resulting in stop codon at 264 |

C

	Parental	505wt	505c6	
140—				◄STAG2
130—				
95—				
72—				
				GAPDH

C-term.
pAb

UM-UC-5

Figure 3-figure supplement 2. Characterization of CRISPR/Cas9-generated *STAG2* knockout in UM-UC-5 bladder cancer cell line. (**A**) sgRNA 505 co-expressed with Cas9 from an all-in-one plasmid was used to generate deleterious frameshift insertions or deletion mutations (indels) in *STAG2* coding exons. The cognate sgRNA target sequence is underlined. Associated protospacer adjacent motifs (PAMs) are marked by boxes. The predicted Cas9 cleavage site is marked by a triangle. (**B**) CRISPR/Cas9-generated *STAG2* indels in the UM-UC-5 cell clone *STAG2*- 505c6 as detected by Sanger sequencing. *STAG2* is located on the X chromosome. Therefore, two alleles had to be inactivated in UM-UC-5 (female) cells. (**C**) Protein lysates prepared from the indicated parental and mutant UM-UC-5 clones were analyzed for STAG2 protein expression by immunoblotting.

A **Restoration of STAG2 expression**
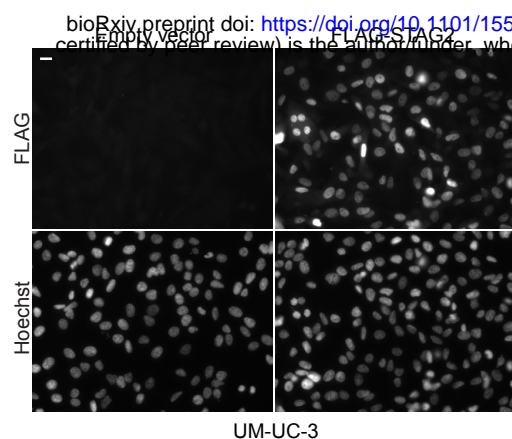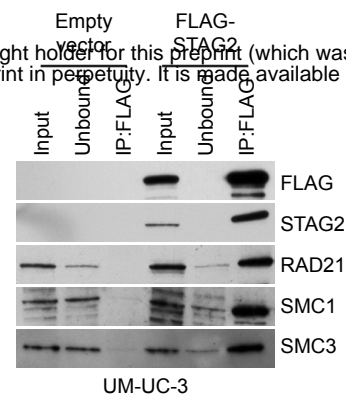
B
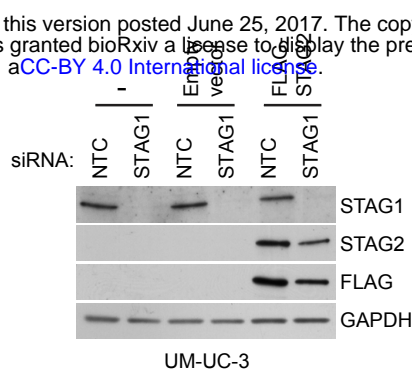
C

Figure 3-figure supplement 3. Restoration of STAG2 protein expression in UM-UC-3 bladder cancer cells. *STAG2*-deficient UM-UC-3 cells were transduced with lentiviral particles encoding no transgene (empty vector) or a 3xFLAG-tagged STAG2 transgene (FLAG-STAG2). Stable selected cell pools were used for further analysis. (**A**) Expression and nuclear localization of the transgenic FLAG-STAG2 protein was assayed by immunofluorescence microscopy. (**B**) Non-transduced UM-UC-3 cells, UM-UC-3 cells transduced with an empty vector and UM-UC-3 cells transduced with a FLAG-STAG2 transgene were transfected with NTC or STAG1 siRNA duplexes. Protein lysates prepared 72 hours after siRNA transfection were analyzed by immunoblotting. (**C**) Protein extracts prepared from UM-UC-3 cells expressing no transgene (empty vector) or a FLAG-STAG2 transgene were subjected to anti-FLAG immunoprecipitation. The input, unbound and precipitated fractions were analyzed by immunoblotting. Co-precipitation of cohesin subunits was only detected in FLAG-STAG2 expressing cells indicating successful incorporation of the transgenic STAG2 protein into the cohesin complex.

van der Lelij, Lieb *et al.* Figure 3-figure supplement 3
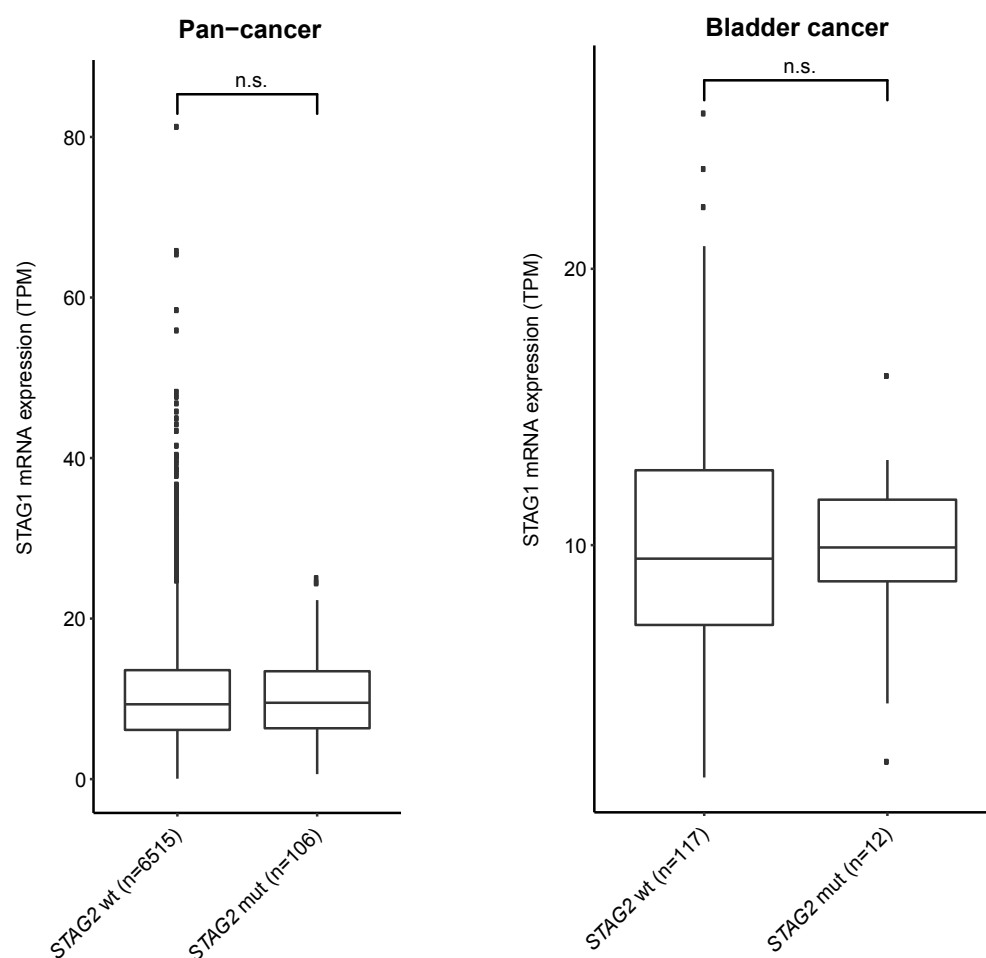
A
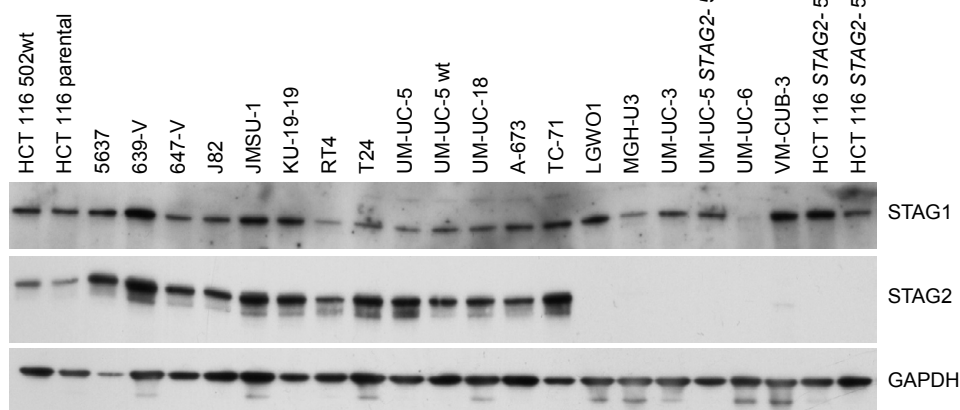
Cancer cell lines

B

Figure 4-figure supplement 1. Analysis of STAG1 protein or mRNA expression in cancer cell lines and patient tumors. **A**, Immunoblot analysis of protein extracts prepared from the indicated cancer cell lines. **B**, STAG1 mRNA expression levels (transcripts per million, TPM) in tumor samples obtained from The Cancer Genome Atlas (TCGA) pan-cancer datasets (left graph) and bladder cancer datasets (right graph). Genetic alteration data were obtained from cBioPortal. The results shown here are in whole or part based upon data generated by the TCGA Research Network: http://cancergenome.nih.gov/. Samples containing alterations resulting in STAG2 amino acid changes (missense mutations, nonsense point mutations or small insertions/deletions) were catagorized as *STAG2* mutated (*STAG2* mut). The boxplot bodies indicate the first quartile (25%), median, and third quartile (75%). The whiskers extend no further than 1.5 times the distance between the first and the third quartiles to the lowest and largest extremes from the boxplot bodies. All samples exceeding the whisker limits are shown individually as points. Significance tests were performed with the wilcox.test function of the ggsignif v0.2.0 R v3.3.2 package. Significance levels were labeled as follows: n.s.>0.05.
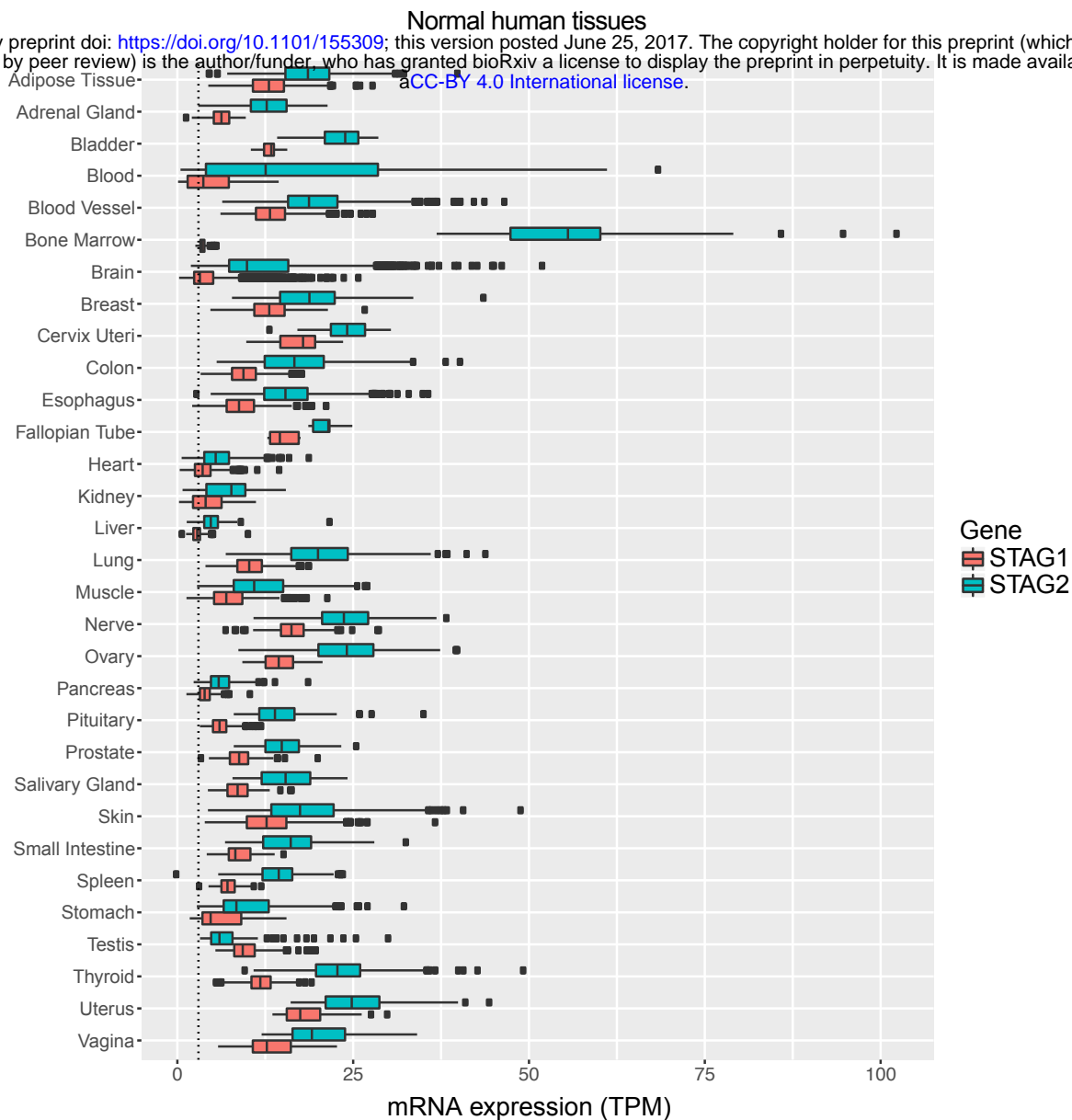
van der Lelij, Lieb *et al.* Figure 4-figure supplement 1

Normal human tissues

Figure 4-figure supplement 2. Expression levels of STAG1 and STAG2 mRNA in normal human tissues. Expression data were obtained from The Genotype-Tissue Expression (GTEx) project (www.gtexportal.org). STAG1 and STAG2 mRNA expression levels (transcripts per million, TPM) in the indicated normal human tissues are plotted. The boxplot bodies indicate the first quartile (25%), median, and third quartile (75%). The whiskers extend no further than 1.5 times the distance between the first and the third quartiles (inter-quartile range, IQR) to the lower and larger extremes from the boxplot bodies. All samples exceeding the whisker limits are shown individually as points. The dotted line indicates a TPM value of 3.

van der Lelij, Lieb *et al.* Figure 4-figure supplement 2